JOURNAL OF SOLID STATE CHEMISTRY **131,** 84–93 (1997)
ARTICLE NO. SC977348

The Surface Structure of the Proton-Exchanged Lithium Manganese Oxide Spinels and Their Lithium-Ion Sieve Properties

K. Sato,[1] D. M. Poojary, and A. Clearfield

Department of Chemistry, Texas A&M University, College Station, Texas 77843-3255

and

M. Kohno and Y. Inoue

Department of Chemistry and Analysis Center, Nagaoka University of Technology, Nagaoka, Niigata 940-21, Japan

Received September 19, 1996; in revised form February 6, 1997; accepted February 14, 1997

The spinel structure and the valence states of the Mn ions both at the surface and the bulk were characterized for the Li^+ extracted and inserted manganese oxide spinels. The Li^+ extraction from the orthorhombic $LiMn_2O_4$ spinel results in the formation of the cubic spinel, the crystal structure of which is the same as λ-MnO_2. The $LiMn_2O_4$ spinel prepared from an electrolytically prepared manganese dioxide is converted to HMn_2O_4 on dilute acid treatment. X-ray photoelectron spectroscopic analysis revealed that the valence state of the surface Mn ions remains unchanged during the Li^+ extraction and insertion, which indicates an occurrence of the Li^+–H^+ ion exchange reaction at the surface irrespective of the solution pH. The Fourier transform infrared photoacoustic spectra of the Li^+ extracted spinel demonstrated the existence of the surface hydroxyl groups, which is considered to be associated with the vacant 8*a* tetrahedral sites in the spinel structure. Based on the thermal stability of the surface hydroxyl groups and the bulk hydroxyl groups, the Li^+ extracted spinel structure is discussed in relation to its lithium-ion sieve property. © 1997 Academic Press

INTRODUCTION

The $LiMn_2O_4$ spinel, in which the Mn_2O_4 framework provides a three-dimensional interstitial space for Li^+-ion transport, maintains its structure over the compositional range $Li_xMn_2O_4$ ($0 \le x \le 1$) by changing the average Mn valency between 3.5 and 4.0 (1, 2). The $LiMn_2O_4$ spinel also shows good electronic conduction due to electron exchanges between Mn^{3+} and Mn^{4+} ions in the octahedral positions of the spinel lattice (3). These structural and electrical features allow the $LiMn_2O_4$ spinel to expand and contract isotropically with electrochemical reduction and oxidation of the Mn ions during lithium insertion and extraction reactions. This property is particularly useful as a cathode material for rechargeable lithium batteries and therefore the electrochemical behavior accompanying structural changes in $LiMn_2O_4$ has been studied extensively so far (4–10). The studies on $LiMn_2O_4$ have been further developed into the synthesis and electrochemical characterization of the stoichiometric spinel compounds, $Li_{1+\delta}Mn_{2-\delta}O_4$ ($0 \le \delta \le 0.33$) (8, 9), in which the average Mn valency varies from 3.5 ($\delta = 0$) to 4.0 ($\delta = 0.33$).

Lithium manganese oxides based on the $LiMn_2O_4$ spinel also possess a lithium-ion sieve property in the aqueous phase after extraction of Li^+ with an acid solution (11–17). The lithium-ion sieve property depends on preparation methods of the starting lithium manganese oxides, the Li/Mn molar ratio, and the heating temperatures which significantly affect the ability of Li^+ incorporation from LiOH solutions (12, 16, 17). As for the Li^+ extraction/insertion reaction, two types of reaction mechanisms have been proposed; one is a redox type (15, 18) and the other is an ion-exchange type (11, 12, 14). Feng *et al.* postulated that the redox-type reaction occurs predominantly for the stoichiometric type of spinel having the $LiMn_2O_4$ composition (17). This mechanism is based on a surface disproportionation reaction of the two trivalent ions (Mn^{3+}) into divalent (Mn^{2+}) and tetravalent (Mn^{4+}) ions, in which the Mn^{2+} ions are soluble in the acid solution under low pH conditions and the Mn^{4+} ions remain in the lattice, forming λ-MnO_2 (18). On the contrary, Shen and Clearfield proposed an ion-exchange mechanism (12). They showed that the Li^+–H^+ ion-exchange form of spinel, HMn_2O_4, in which the number of Mn^{3+} and Mn^{4+} remains unchanged throughout the reaction, has a high

[1] On leave from Nagaoka University of Technology. Present address: Analysis Center, Nagaoka University of Technology, Nagaoka, Niigata 940-21, Japan. E-mail: sato@analysis.nagaokaut.ac.jp.

0022-4596/97 $25.00
Copyright © 1997 by Academic Press
All rights of reproduction in any form reserved.

specificity for Li^+ with complete reversibility in Li^+–H^+ ion-exchange. The Li^+–H^+ ion-exchange reaction is also likely to occur in spinels with increased number of tetravalent Mn ions (17), i.e., $Li_{(1+\delta)}Mn_{(2-\delta)}O_4$ with increasing value of δ up to 0.33. Proton sites in the manganese oxide spinel, the stoichiometric composition of which is based on $Li_4Mn_5O_{12}$ ($\delta = 0.33$), have therefore been characterized recently with the inelastic neutron scattering (INS) technique (19). This study showed that in the spinel lattice the inserted protons can exist in the form of hydroxyl groups and structural water molecules, which are associated with the vacant 8*a* tetrahedral sites and oxygen atoms at 16*d* octahedral vacancies, respectively.

However, the reason for the high specificity for the lithium-ion sieve properties of the spinel-type lithium manganese oxides remained uncertain in relation to their crystal structures and the valence states of the Mn ions. Thus, we have undertaken a detailed study on the characterization of the structural change of the $LiMn_2O_4$ spinel during the Li^+ extraction/insertion reactions. In addition to the lithium-ion sieve property, the Li^+-extracted $LiMn_2O_4$ spinel has a high catalytic activity for the oxidation of methane and butane, in which valence states of the Mn ions at the surface of the catalyst play an important role (20, 21).

We therefore investigated the spinel structure and the valence states of the Mn ions both at the surface and in the bulk for Li^+-extracted manganese oxide spinels to see the effect on the lithium-ion sieve property of these spinels.

EXPERIMENTAL

Sample Preparation

$LiMn_2O_4$ spinel was prepared by solid state reaction of α-Mn_2O_3 (Soekawa, 99.9% in purity) and Li_2CO_3 (Wako, 99.9% in purity) mixed in a molar ratio of 2 : 1. The powder was put in an alumina crucible after mixing in an agate mortar and then heated in air at 850°C for 2 to 20 h followed by air cooling. To check incorporation of impurities during the heating process, the sample heated for 4.5 h was analyzed with a JEOL Model 733 electron microprobe analyzer, operating at an accelerating voltage of 25 kV, equipped with an energy dispersive X-ray spectrometer which can detect elements with higher atomic numbers than ^{11}Na. The X-ray spectra showed that any elements other than Mn in the sample were not detected within the detection limit of the X-ray spectrometer. This analysis indicates an occurrence of no appreciable contamination from the crucible during the heating process. Morphology of the powder samples was observed with a scanning electron microscope attached on the electron microprobe analyzer. As manganese oxide sources, $MnCO_3$ (Baker, 99.9% in purity) and MnO (Strem, 99% in purity) were also used to identify the spinel phase formed. A mixture of $MnCO_3$ or MnO with Li_2CO_3 was respectively heated in air at 850°C for 2 to 20 h.

Li^+ extraction was made for a 2 g sample of the $LiMn_2O_4$ spinel prepared from a mixture of Mn_2O_3 and Li_2CO_3 heated for 4.5 h. The sample was stirred in a HNO_3 solution of 100 ml with different concentrations each at room temperature for 5 h. The amount of extracted lithium ions was determined from the lithium concentration in the HNO_3 solution, which was measured with a Shimazu Model 646 atomic absorption spectrometer. The acid-treated sample was filtered, washed with distilled water, and dried at 80°C. Surface areas of the samples were measured by the Brunauer, Emmett, and Teller (BET) method using nitrogen gas. Before the surface area measurement, each sample, weighing about 0.5 g, was heated in air to 150 or 200°C, depending on the thermal stability of samples, for at least 10 h and then degassed under vacuum at 100°C for 16 h. For comparison, Li^+ extraction was made for a lithium-ion-exchanged manganese dioxide, which had been electrolytically prepared from a solution of $MnSO_4$ and H_2SO_4. Prior to the Li^+ extraction the ion-exchanged manganese dioxide was heated at 520°C. The extraction was made in a 0.1 *N* HNO_3 solution at room temperature for 24 h. Further experimental details are described in Ref. (12).

Determination of the Average Mn Valency

The average Mn valencies of the Li^+-extracted samples, consisting of trivalent and tetravalent Mn ions, were determined by the phase analysis of manganese oxides (22) combined with the chemical titration method (23). A 0.50 g sample was treated with a mixture of 2 *N* H_2SO_4 and 48% HF in a volume ratio of 2:1 to dissolve the trivalent manganese oxide component, Mn_2O_3. The residue from the trivalent manganese solution was analyzed for the tetravalent manganese oxide component, MnO_2. The residue was weighed after drying in air at 120°C for 12 h and then stirred at 55°C in a solution of 0.1 *N* ferrous ammonium sulfate ($FeSO_4(NH_4)_2SO_4 \cdot 6H_2O$) and 3 *N* H_2SO_4 until the sample was completely dissolved. The excess $FeSO_4$ $(NH_4)_2SO_4$ was titrated with a 0.1 *N* $KMnO_4$ solution to determine the equivalent amount of MnO_2 that had been incorporated in the sample. Due to the sample loss, which might have occurred during the filtration, the relative experimental error for the determination of the average Mn valency was estimated to be ± 0.05.

Potentiometric Titration

Potentiometric titration was carried out in polyethylene bottles using 50 mg of the acid-treated $LiMn_2O_4$ sample prepared from Mn_2O_3 and Li_2CO_3. Each weighed sample was immersed in 10 ml of 0.05 *M* (LiCl + LiOH) solution in varying ratio and intermittently shaken at 25°C for 3 days.

The pH of the solution after the titration was measured with a Corning 200 pH meter. The lithium concentration of the solution was also determined after the titration by atomic absorption spectroscopy.

Sample Characterization

Step scanned X-ray powder diffraction data for the sample were collected on the finely ground sample. The X-ray source was a Rigaku rotating-anode generator operating at 50 kV and 180 mA with a copper target and graphite monochromator. The data were collected in the 2θ range 15°–90° with a step size of 0.01° and a count time of 10 s per step. Rietveld refinement of the full pattern was carried out in the program GSAS (24).

Thermogravimetric analysis (TGA) was made with a horizontal-type Dupont Model 951 TG analyzer at a heating rate of 3°C min^{-1} in air and differential thermal analysis (DTA) was made with a Dupont Model 910 DT analyzer at a heating rate of 10°C min^{-1} under flowing nitrogen gas atmosphere at a rate of 50 ml min^{-1}. The TG and DTA measurements were made for approximately 50 mg samples.

XPS analysis was performed with a PHI Model 550 photoelectron spectrometer using a Mg$K\alpha$ X-ray source ($h\nu = 1253.6$ eV), powered at 15 kV and 40 mA. The residual pressure in the spectrometer during the measurements was in the range from 2×10^{-6} to 5×10^{-6} Pa. As an internal standard of the samples a binding energy of 284.9 eV was taken for the C 1*s* peak. Atomic concentration ratios were calculated by correcting the intensity ratios with the theoretical sensitivity factors based on the Scofield cross sections (25), assuming the transmission function of the spectrometer to be independent of the kinetic energy. Before the XPS analysis, the sample powders were heated in air at 100°C for overnight and subsequently pressed into a thin disk.

Photoacoustic spectra were recorded on a JASCO FT/IR-500 spectrometer modified for acoustic detection with an MTEC photoacoustics Model 200 detector. The single-beam spectrum of each sample was obtained at a mirror velocity of 2 mm s^{-1}. For a correction of the light source and instrument profiles, a carbon black spectrum was used as a background spectrum. To reduce background signals generated in the detector, all spectra were obtained after purging for 5 to 10 min with dry helium gas. Photoacoustic spectra were thus obtained for both as-prepared and heat-treated samples. The heat treatment was made in air at 150°C for 1 h. The heat-treated samples were subsequently transferred into the photoacoustic detector using a table-top glove box filled with helium atmosphere. Usual infrared spectra were also obtained with a BIO-RAD FTS-40 spectrometer by the KBr disk technique on samples heated from 25 to 300°C at a heating rate of about 10°C min^{-1} in flowing nitrogen gas atmosphere. The infrared absorption spectra were recorded at temperatures up to 300°C.

RESULTS

$LiMn_2O_4$ Spinel Formation

The X-ray diffraction profiles revealed that the solid state reaction between Mn_2O_3 and Li_2CO_3 powders at 850°C yields a spinel phase for the reaction time of at least 2 h. The formation of the spinel phase was accompanied by the disappearance of reflections from the reactants. Figure 1 shows a comparison of X-ray diffraction profiles for the spinel phases that appeared at heating times of 4.5 and 20 h. Enlarged profiles around $2\theta = 44°$ are shown in Fig. 2. The profile shown in Fig. 1a is assigned to an *F*-centered orthorhombic cell with a slight difference in its lattice parameters, $a = 8.2692(4)$ Å, $b = 8.2468(4)$ Å, and $c = 8.2205(3)$ Å. The profile shown in Fig. 1b is assigned to an *F*-centered cubic cell with the lattice parameter, $a = 8.238$ Å. In addition to the reflections that can be indexed, small extra reflections were observed in both samples at $2\theta = 28.9°$ ($d = 3.09$ Å)

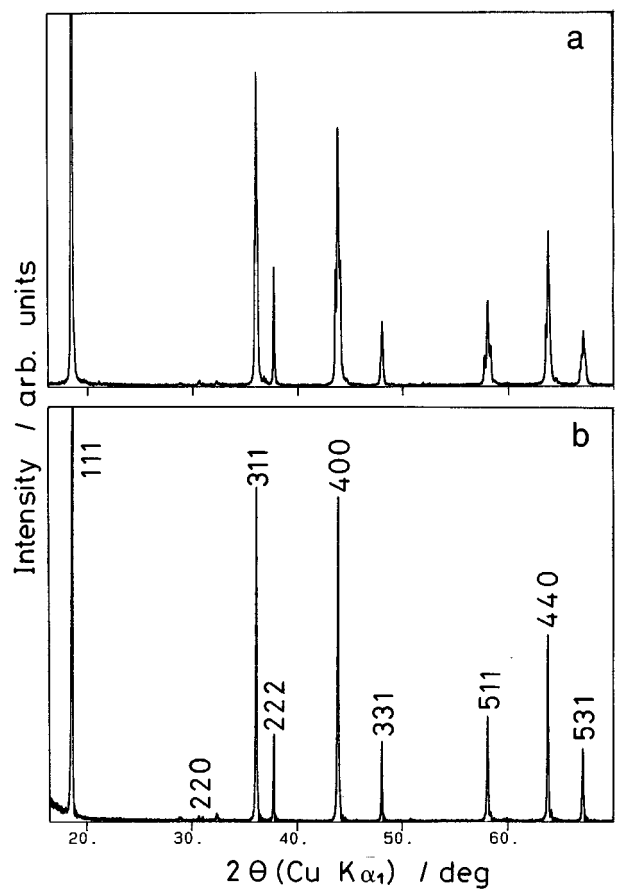

FIG. 1. X-ray diffraction profiles of the $LiMn_2O_4$ spinels prepared by solid state reaction between Mn_2O_3 and Li_2CO_3 heated at 850°C for (a) 4.5 h and (b) 20 h.

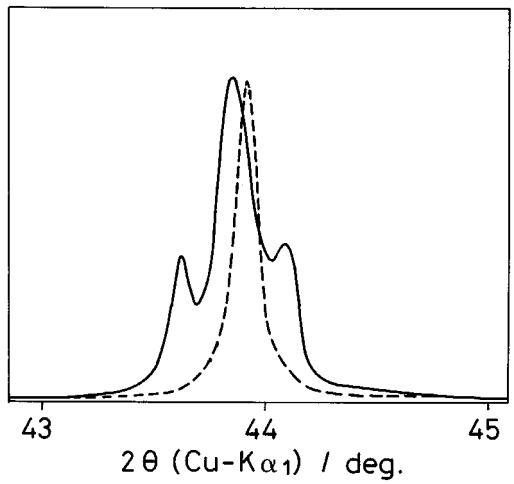

FIG. 2. Enlarged X-ray diffraction profiles around the 400 reflection of the $LiMn_2O_4$ spinels prepared from Mn_2O_3 and Li_2CO_3. The solid line shows the sample heated for 4.5 h and the dotted line shows the sample heated for 20 h.

and 32.7° ($d = 2.74$ Å). These reflection lines are ascribed to 112 ($d = 3.089$ Å) and 103 reflections ($d = 2.768$ Å) from the tetragonal Mn_3O_4 phase (26). The 211 reflection ($d = 2.487$ Å), which has the intensity ratio of 100 : 85 to the 103 reflection in the tetragonal Mn_3O_4, is overlapped with the 311 reflection in $LiMn_2O_4$. The X-ray diffraction profiles of the MnO–Li_2CO_3 and $MnCO_3$–Li_2CO_3 mixtures heated at 850°C showed formation of the single cubic spinel phase without forming the orthorhombic spinel phase. These results indicate that formation of the orthorhombic $LiMn_2O_4$ spinel is specific to the early stages of the solid state reaction between Mn_2O_3 and Li_2CO_3.

TABLE 1
Crystallographic Parameters of Orthorhombic $LiMn_2O_4$ Spinel

Atom	Position	x	y	z	B (Å^2)
Li	8*a*	0.125	0.125	0.125	1.4(1)
Mn	16*d*	0.5	0.5	0.5	2.6(3)
O	32*h*	0.257(1)	0.267(1)	0.258(1)	1.2(2)

Note. R factors: $R_p = 14\%$, $R_{wp} = 17.9\%$, $R_F = 3.99\%$ (for 116 reflections). Occupancy factors: Li, 1.13(2); Mn, 1.00(1). Space group, *Fddd* (No. 70); $a = 8.2692(4)$ Å , $b = 8.2468(4)$ Å, $c = 8.2205(3)$ Å

The structure of the orthorhombic $LiMn_2O_4$ spinel was refined with X-ray diffraction data in the space group *Fddd*. The lithium ions were positioned on the 8*a* tetrahedral sites (site symmetry 222), the manganese ions on the 16*d* octahedral sites (on center of symmetry), and the oxygen ions on the 32*h* sites (general position). The refined crystallographic parameters are summarized in Table 1. The observed and calculated X-ray diffraction profiles are shown in Fig. 3.

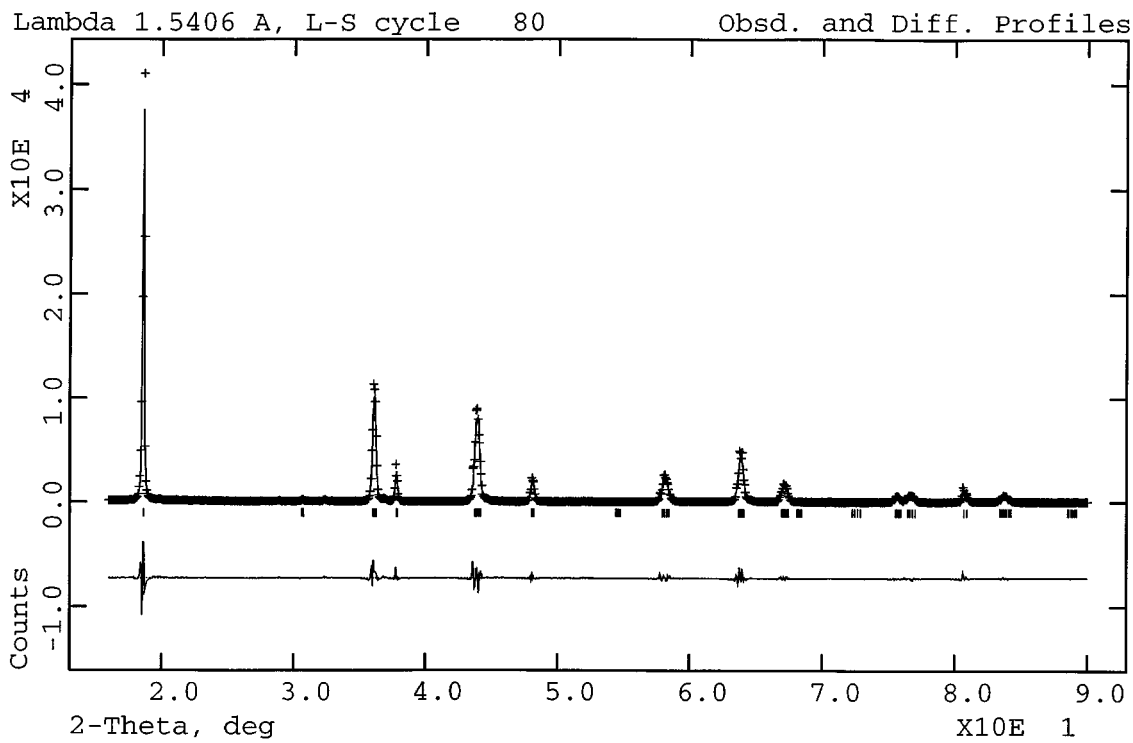

FIG. 3. Observed (crossed marks) and calculated (solid line) X-ray diffraction profile for the $LiMn_2O_4$ spinel prepared from Mn_2O_3 and Li_2CO_3 heated in air at 850°C for 4.5 h. The difference between observed and calculated profiles is plotted below.

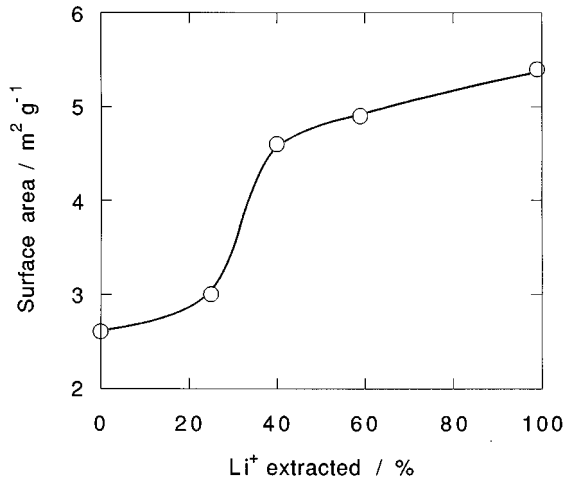

FIG. 4. Variation of surface area with the Li^+ extraction from the orthorhombic $LiMn_2O_4$ spinel.

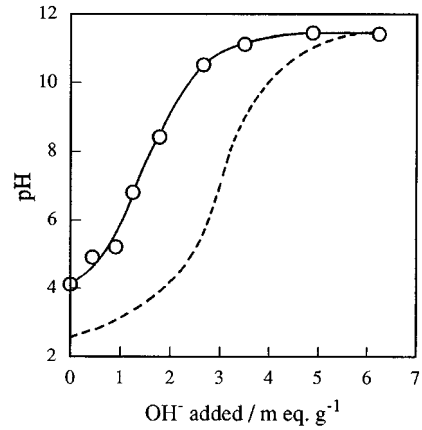

FIG. 5. Titration curve for the Li^+ extracted sample prepared from the orthorhombic $LiMn_2O_4$ spinel (sample A). The broken line shows the titration curve, taken from Ref. (12), for the exchanger prepared from electrolytically prepared manganese dioxide (sample B).

The structure analysis yielded a composition close to the stoichiometric spinel $(Li_{1.0})_{8a}(Mn_{2.0})_{16d}O_4$.

The Extraction and Insertion of Lithium Ions

Treating the starting material, the orthorhombic $LiMn_2O_4$ spinel, with a 1 *N* HNO_3 solution removed 99% of the lithium ions and formed a cubic spinel phase (sample A), which was identified by nonsplitting reflection peaks in the X-ray diffraction profile. The average Mn valency of sample A was determined to be 3.9. We further confirmed that the amount of lithium ions extracted from the starting material increased with increasing HNO_3 concentration; treatment with solutions of 0.1 and 0.5 *N* concentrations results in removal of 40 and 95% lithium from the starting $LiMn_2O_4$ material, respectively. Figure 4 shows the variation of the surface area with Li^+ extraction. The surface area of the starting material, 2.6 m^2 g^{-1}, was increased to 5.4 m^2 g^{-1} by the completion of Li^+ extraction. The average particle size of the starting material, estimated from electron micrograph distributions, was about 0.5 μm in its cubic shape. After the 99% Li^+ extraction, the average particle size reduced to about 0.3 μm and the particles changed into somewhat round shapes with a tendency toward agglomeration. The X-ray diffraction profile of sample A showed rather broad reflections from the cubic structure compared to that observed for the starting material and the lattice parameter of sample A was found to be 8.03 Å. By comparison, treating the Li^+-incorporated manganese dioxide with a 0.1 *N* HNO_3 solution removed more than 99% of lithium ions and formed a proton-exchanged spinel (sample B), the average Mn valency of which was determined to be 3.5. The X-ray diffraction profile of sample B showed only diffuse reflections of 111, 311, and 400, which could be indexed on the basis of a cubic unit cell. The above results are summarized in Table 2.

Figure 5 shows the measured potentiometric titration curve of sample A in comparison with the curve of sample B, which was taken from Ref. (12). These curves indicate that the exchange capacity of sample A was smaller than that of sample B over the pH range examined. Furthermore, the atomic absorption analysis of the titrated solution revealed that the actual exchange capacity of sample A at pH 12 was

TABLE 2
Properties of the Li^+ Extracted Samples

Material	%Li extracted	Average Mn valency	Surface area (m^2 g^{-1})	Lattice parameter *a* (Å)
Sample A	99.0	3.9	5.4	8.03
Sample B	> 99	3.5	43.4[a]	8.08[b]
$LiMn_2O_4$[c]	0	3.5	2.6	8.2692

[a] Determined from the electrolytically prepared condition.
[b] Estimated from the value of the d_{400} spacing.
[c] Prepared from Mn_2O_3 and Li_2CO_3 heated at 850°C for 4.5 h.

3.60 meq g^{-1}, a value that is lower than that of sample B, 4.63 meq g^{-1}.

Sample Characterization

Figures 6 and 7 show TG and DTA curves for sample A and sample B, respectively. The TG curve of sample B showed a significant weight decrease, 14 wt%, up to approximately 140°C. This is mainly caused by the desorption of adsorbed water as indicated by the endothermic peak in the DTA curve at 70°C. The TG curve of sample A showed a slight weight decrease, 0.6 wt%, up to 200°C. This slight decrease is in accordance with the DTA results, which did not exhibit any detectable endothermic peak up to 200°C. Following the first rapid decrease in weight, both samples showed an exothermic peak. The temperature of the exothermic peak, 260°C, observed for sample A is higher than that, 205°C, for sample B. Sample A and sample B exhibited the transformation from the spinel phase to the β-MnO_2 phase after passing each exothermic peak. The formation of the β-MnO_2 phase was confirmed by the X-ray diffraction profiles of the samples heated to 350°C. In addition, the DTA curve of sample B showed a very broad exothermic tendency, whose maximum peak was observed around 300°C. With further heating, the β-MnO_2 phase, which appeared in both sample A and sample B, transformed into the Mn_2O_3 phase at around 550°C.

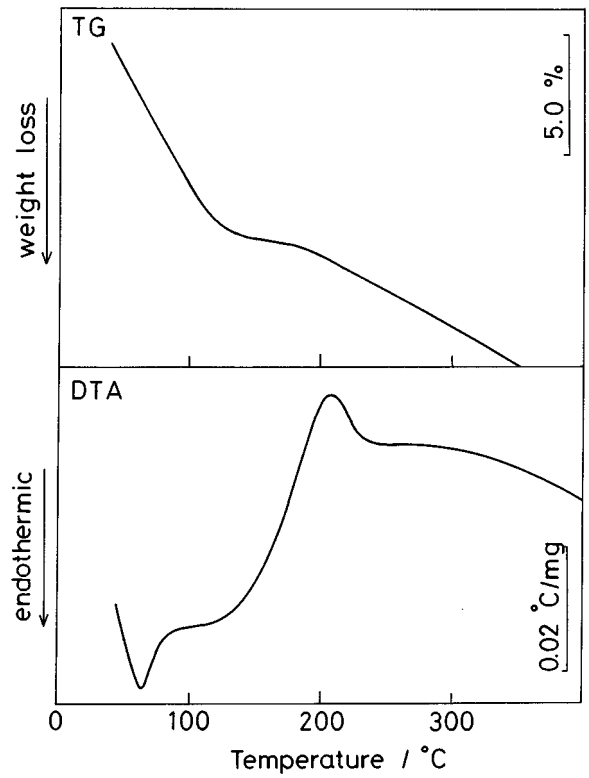

FIG. 7. TG and DTA curves for proton-exchanged HMn_2O_4 prepared from electrolytically prepared manganese dioxide (sample B).

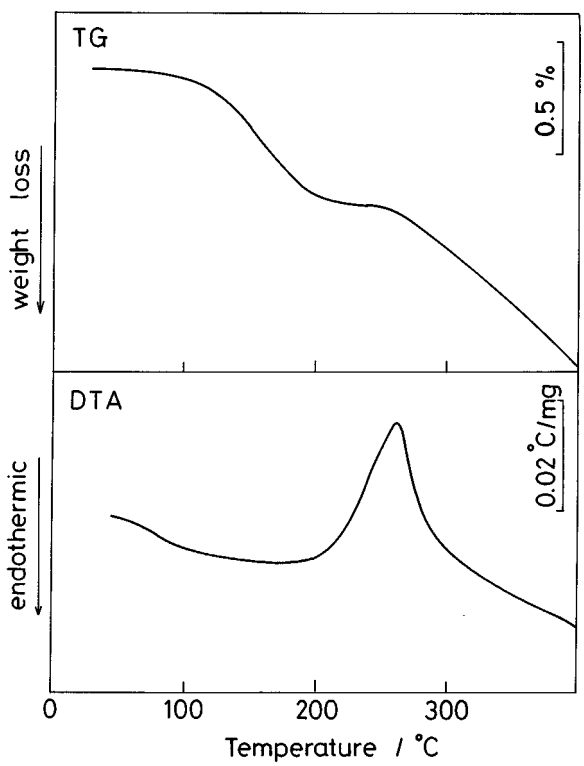

FIG. 6. TG and DTA curves for the Li^+ extracted sample (sample A).

Figure 8 shows the XPS spectra of the Mn 3*s* level measured in the binding energy range 80–93 eV. Since Mn ions have unpaired electrons, the Mn 3*s* peak gives a doublet ascribable to multiplet splitting (27). The separation widths of the doublet peak for the lithium extracted materials, sample A and sample B, were 5.0 eV, whereas the separation width for the β-MnO_2 sample, which had been formed from sample A by heating to 350°C, was 4.4 eV. This indicates that the surface valence states of sample A and sample B are lower than that of β-MnO_2, whose average Mn valency is four. The separation width was also measured for the starting material, $LiMn_2O_4$, and for sample A where Li^+ has been reinserted by treatment with 0.05 *M* LiCl–LiOH solution at pH 8.4 (see Fig. 5). The measured values were 5.0 eV for both materials. These results show that the surface valency of Mn for sample A and sample B is 3.5, which is the same value as that of the $LiMn_2O_4$ spinel and is not changed by the lithium reinsertion. This implies that neither removal nor incorporation of lithium ions in the reaction studied affects the surface valence state of the Mn ions. Note the difference between the valency determined by the XPS analysis and that determined by chemical analysis for the bulk of the samples shown in Table 2. The XPS analysis of the O 1*s* and Mn 2*p* spectra for sample A, sample B, and the

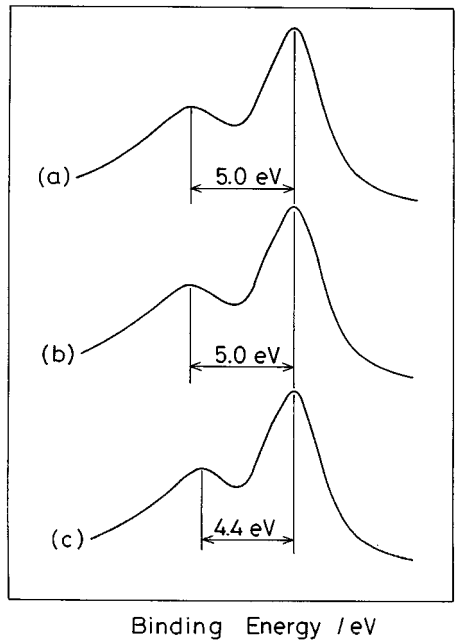

FIG. 8. X-ray photoelectron spectra of the Mn 3*s* for (a) the Li^+ extracted sample (sample A), (b) proton-exchanged HMn_2O_4 prepared from electrolytically prepared manganese dioxide (sample B), and (c) β-MnO_2. The β-MnO_2 in (c) was prepared from sample A heated to 350°C.

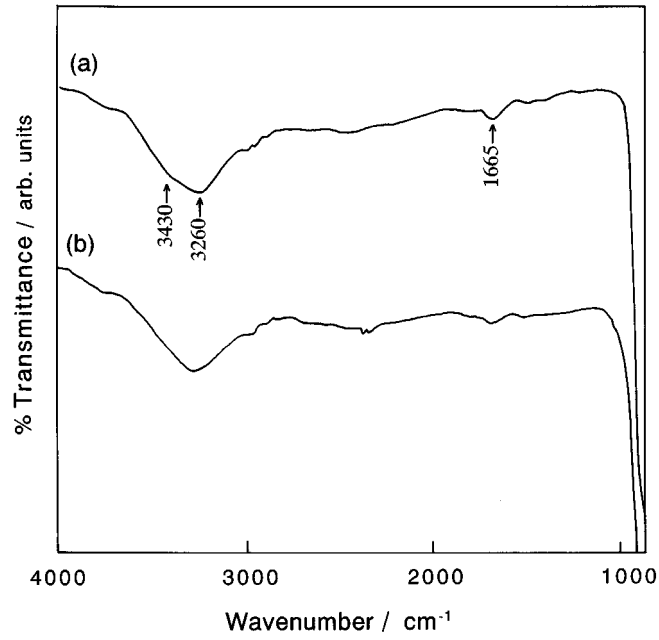

FIG. 9. Infrared spectra of the Li^+ extracted sample (sample A) at (a) 90°C and (b) 300°C. The spectra in the wavenumber below 1000 cm^{-1} were not obtained due to the absorption effect by the window of the heating unit.

samples before the acid treatment showed that the O/Mn atomic concentration ratio, 2.0, remains constant. The Li 1*s* spectra, which were identified at 54.5 eV before the acid treatment, were not identified for sample A and sample B.

The infrared absorption spectra of sample A dispersed in KBr disks are shown in Fig. 9. The spectra obtained at 90 and 300°C in the range 1000–4000 cm^{-1} show the OH bending vibration between 1500 to 1700 cm^{-1} and the OH streching vibration above 3200 cm^{-1}. These spectra show that significant changes were not observed by heating in KBr up to 300°C except a slight decrease in intensity of the shoulder positioned at 3430 cm^{-1}. The band at 3430 cm^{-1} has been ascribed to a streching vibration of the lattice hydroxyl group, and this band is distinctly observed for the Li^+-extracted samples prepared from the $Li_{(1+\delta)}Mn_{(2-\delta)}O_4$ spinel, the composition of which is close to $\delta = 0.33$ ($Li_4Mn_5O_{12}$) (17).

Fourier transform infrared photoacoustic spectroscopy (FT-IR-PAS) was used to draw surface-sensitive information (28) on the lattice hydroxyl group from the Li^+ extracted spinel without affecting the sample morphology. Figure 10 shows the FT-IR-PAS spectra obtained for the orthorhombic $LiMn_2O_4$ spinel and its Li^+ extracted form (sample A). PAS signals correspond to infrared transmission signals at the same wavelengths. The FT-IR-PAS spectra of sample A dried at 80°C, shown in Fig. 10b, include an intense band at 910 cm^{-1}, which was not clearly identified in sample A with the usual IR spectra. The same FT-IR-PAS spectra also include distinct bands at 1640 and 3350 cm^{-1}, and this is in contrast to the weak bands observed for the starting $LiMn_2O_4$ spinel, shown in Fig. 10a, in the range between 1500 and 1700 cm^{-1} and above

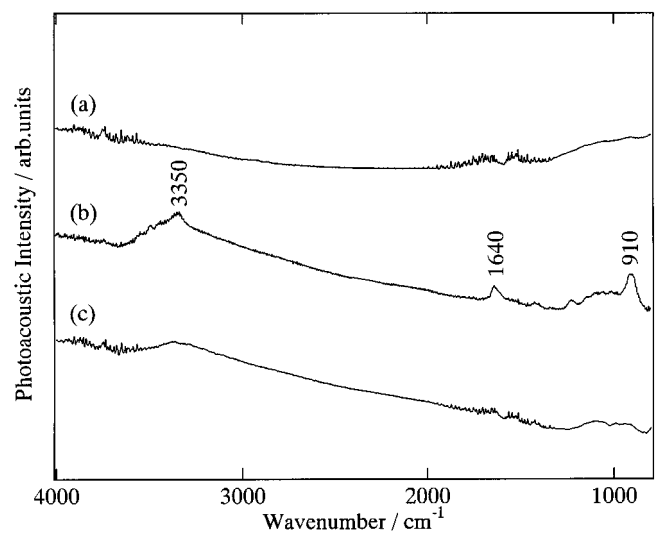

FIG. 10. Fourier transform infrared photoacoustic spectra of (a) the orthorhombic $LiMn_2O_4$ spinel, (b) the Li^+ extracted sample (sample A) dried at 80°C, and (c) sample A after heating at 150°C for 1 h.

3200 cm^{-1}. The band at 910 cm^{-1} observed for sample A is ascribed to a lattice coupling vibration of hydroxyl groups (17, 19). This band was not observed in the starting $LiMn_2O_4$ spinel irrespective of heating. Figure 10c shows that heating sample A to 150°C results in a disappearance of the band at 910 cm^{-1} and a decrease in intensity of the bands at 1640 and 3350 cm^{-1} though the spectra contain an effect of residual H_2O in the spectrometer, which was difficult to eliminate. The disappearance of the band at 910 cm^{-1} indicates that the lattice protons are desorbed by heating. A decrease in intensity of the spectra between 960 and 1300 cm^{-1} was also observed with a disappearance of the weak band at 1220 cm^{-1} after heating to 150°C, so that this band is most likely to be related to a hydroxyl deformation mode (19).

DISCUSSION

Formation of the Orthorhombic $LiMn_2O_4$ Spinel

In the isothermal cross section of the ternary Li–Mn–O system established at 25°C (8, 9), the $LiMn_2O_4$ phase exists with the Mn_3O_4 phase on the tie-line between $LiMn_2O_4$ and Mn_3O_4. As shown in Fig. 1, the existence of a slight amount of Mn_3O_4 with the spinel phase indicates that the lithium manganese oxide identified in the present experiment, being in equilibrium with Mn_3O_4 at the heating temperature, has the stoichiometric $LiMn_2O_4$ composition. The reaction between α-Mn_2O_3 and Li_2CO_3 at 850°C for more than 4.5 h results in formation of the cubic $LiMn_2O_4$ spinel, which is thermodynamically stable, via a metastable orthorhombic spinel. The formation of the orthorhombic $LiMn_2O_4$ spinel was found to be specific to the initial stages of the powder reaction between the reactants of α-Mn_2O_3 and Li_2CO_3. In the case of powder reactions, the reaction kinetics are controlled by many parameters, such as grain size distribution, grain shape, contact area between the grains, and melting point and vapor pressure of the reactants. Furthermore, in solid state powder reactions growth of the reaction product occurs at contact points of the grains. Li_2CO_3 starts to melt at 618°C so that melting of the Li_2CO_3 powders, accompanying decomposition into Li_2O, is considered to provide a uniform supply of the lithium oxide reactant over the entire surface of α-Mn_2O_3 grains at the reaction temperature of 850°C. This will effectively allow the powder reaction of $LiMn_2O_4$ formation from α-Mn_2O_3 and Li_2CO_3 to proceed.

Among the reaction mechanisms proposed for the spinel formation reaction (29), two mechanisms can be considered for $LiMn_2O_4$ spinel formation. One is mutual migrations of lithium and manganese ions through the sublattice of oxygen ions and the other is simultaneous diffusion of lithium ions and electrons to the $LiMn_2O_4/Mn_2O_3$ interface with a concurrent supply of oxygen through the gas phase. In the present case, the latter mechanism is probable since the diffusion of the lithium ion is considered to be faster than that of the manganese ion and $LiMn_2O_4$ has high electronic conductivity (3). This is explained in view of the crystal structure of α-Mn_2O_3. In the structure of α-Mn_2O_3, the oxygen ions can occupy cubic close-packed positions as a spinel-type structure. However, lack of one-quarter of the oxygen ions in the lattice yields a slightly distorted arrangement of the oxygen ions for the octahedral coordination of the Mn ions (30). Thus, α-Mn_2O_3 has the orthorhombic structure with the lattice parameters $a = 9.4161$ Å, $b = 9.4237$ Å, and $c = 9.4051$ Å (31). Due to the similarity in crystal structure of α-Mn_2O_3 to that of the spinel, the orthorhombic $LiMn_2O_4$ spinel can be formed by the diffusion of lithium ions with a concurrent supply of oxygen ions into the α-Mn_2O_3 framework at the initial stages of the spinel formation reaction.

Extraction and Insertion of Lithium Ions

We confirmed that extraction of 99% Li^+ from the orthorhombic $LiMn_2O_4$ spinel with a 1 *N* HNO_3 solution forms a cubic spinel with the lattice parameter $a = 8.03$ Å and the average Mn valency close to 4, i.e., sample A. This structure is the same as λ-MnO_2. Furthermore, with increased HNO_3 concentration from 0.05 to 1 *N*, the surface area of the Li^+-extracted sample increased probably due to the dissolution of Mn^{2+} into the acid solution and, accordingly, this is accompanied by a particle size reduction. These results support the idea that surface disproportionation reaction, $2Mn^{3+} \rightarrow Mn^{4+} + Mn^{2+}$, in acid solutions at pH < 2 is responsible for the formation of λ-MnO_2 (18). The surface disproportionation mechanism is rational because the shift of the point of zero zeta potential (p.z.z.p.) for $LiMn_2O_4$ to lower pH with Li^+ extraction (1) can qualitatively well explain the relation between the amount of extracted Li^+ and the pH of the acid solution. The pH of p.z.z.p. for the orthorhombic $LiMn_2O_4$ spinel is probably the same as for the cubic spinel since the Li^+ extraction behavior from the orthorhombic $LiMn_2O_4$ spinel and the structure of the resulting product is the same as that of the cubic $LiMn_2O_4$ spinel. The similarity of the titration curve, shown in Fig. 5, to the curve for λ-MnO_2 (17) could support this. Thus, a slight distortion in the lattice Mn_2O_4 framework of the starting material does not affect the Li^+ extraction process and the structure of the product.

The XPS analysis of the Mn 3*s* peaks showed that the average valency of the surface Mn ions in both sample A and sample B is 3.5; equal numbers of Mn^{3+} and Mn^{4+} ions exist at the surface of the Li^+-extracted samples. Since lithium was not detected at the surfaces of sample A and sample B, the XPS result indicates that the surface oxygens are associated with protons, forming hydroxyl groups and remaining the same valence state of the Mn ions as that of

$LiMn_2O_4$. Thus we can conclude that the surface composition of sample A is HMn_2O_4. In the surface disproportionation mechanism (18), the electrons that migrated from the interior of the particle reduce the surface Mn^{3+} ions to Mn^{2+} ions with simultaneous formation of water from the surface O^{2-} ions with protons in the acid solution. If protons adsorbed on the surface of the particle exchange with the surface lithium ions before the Mn^{2+} dissolution, surface hydroxyl groups will be formed. The observation of the hydroxyl group on the FT-IR-PAS spectra supports the plausibility of the predominant Li^+/H^+ ion-exchange mechanism at the surface of $LiMn_2O_4$. However, transport of protons to the interior of the particle accompanying an exchange with Li^+ ions will not be easy through the three-dimensional arrays of the spinel lattice, unless there exists vacancies at the 16*d* octahedral sites as in $Li_4Mn_5O_{12}$, whose Mn valency is 4. We therefore infer that the dissolution reaction takes place when the excess protons adsorbed on the surface of $LiMn_2O_4$ from an acid solution attract electrons from the interior of the particle to reduce the surface Mn^{3+} to Mn^{2+}. This situation is accomplished only at low pH conditions.

The transmission infrared spectra of λ-MnO_2 samples prepared from $LiMn_2O_4$ do not clearly show the existence of lattice hydroxyl groups, whereas the spectra of the proton-inserted spinels prepared from the starting spinel composition close to $Li_4Mn_5O_{12}$ clearly show the existence of lattice hydroxyl groups (17). The spectra in proton-inserted spinels of composition close to $H_{1.33}Mn_{1.67}O_4$ ($=H_4Mn_5O_{12}$) show an intense band at 910 cm^{-1} that is assigned to a lattice coupling vibration of hydroxyl groups associated with the vacant 8*a* tetrahedral sites (19), but the spectra in the λ-MnO_2 samples do not show this band. These findings indicate that the amount of bulk hydroxyl species in sample A, λ-MnO_2, is very small. By comparison, lattice hydroxyl groups, or structural water, in the proton-inserted spinels are removed by heating above 150°C with concurrent destruction of the spinel lattice (19). The similarity in the disappearance of the surface hydroxyl groups observed for sample A in the FT-IR-PAS spectra to that of the lattice hydroxyl groups indicates that the structural water also exists at the surface of sample A. The concurrent decrease in the FT-IR-PAS spectrum of the water absorption at around 1640 and 3430 cm^{-1} with heating to 150 °C also supports this. Different from the cases of γ-MnO_2 (32) and the proton-inserted spinels prepared from $Li_4Mn_5O_{12}$ (19), removal of the surface protons and/or the structural water from sample A results in oxidation of the surface Mn ions toward the tetravalent state without destructing the spinel structure up to about 200°C. This was confirmed with the XPS analysis and temperature programmed desorption spectra of H_2^+ for sample A (20), and in good agreement with the TG-DTA curves in Fig. 6.

In contrast, sample B has an almost completely proton-exchanged form without dissolution of Mn^{2+} ions after the treatment in a 0.1 *N* HNO_3 solution. Sample B also shows an excellent reversibility in the titration reactions. These properties show that the acidity of sample B is stronger than that of sample A due to the incorporation of protons into the bulk. The proton-insertion mechanism has been already discussed by Shen and Clearfield (12). The DTA curve of sample B, shown in Fig. 7, indicates that the protons are loosely bound to the lattice oxygens so that they can easily desorb at lower temperatures and the transformation temperature to the β-MnO_2 phase becomes lower than that of λ-MnO_2 by approximately 50°C. The incomplete crystallization or the nanometer-level crystalline state and the small grain size with large surface area can result in the occurrence of the complete Li^+–H^+ ion-exchange reaction at low pH without the dissolution of the oxide.

CONCLUSIONS

Li^+ extraction from the orthorhombic $LiMn_2O_4$ spinel and the electrolytically prepared $LiMn_2O_4$ spinel with a HNO_3 solution results in formations of λ-MnO_2 (sample A) and HMn_2O_4 (sample B), respectively. Slight distortion of the Mn_2O_4 framework in the orthorhombic structure does not affect the formation of λ-MnO_2; the λ-MnO_2 product prepared in a 1 *N* HNO_3 solution has a cubic structure with the lattice parameter 8.03 Å. The valence states of the surface Mn ions in λ-MnO_2 and HMn_2O_4 are the same as that in the starting $LiMn_2O_4$, which indicates an occurrence of the Li^+–H^+ ion exchange reaction at the surface. However, the valence states of the bulk Mn ions determined by chemical analysis are 3.9 for sample A (λ-MnO_2) and 3.5 for sample B (HMn_2O_4). Thus, the surface disproportionation reaction, $2Mn^{3+} \rightarrow Mn^{4+} + Mn^{2+}$, for forming λ-MnO_2 must involve the exchanged protons at the surface as well as the adsorbed protons from the acid solution. The surface hydroxyl groups observed for λ-MnO_2 are considered to be associated with the vacant 8*a* tetrahedral sites in the spinel structure and exist in the same form as lattice hydroxyl groups. The exchanged protons are not transported from the surface to the interior through the three-dimensional arrays in the λ-MnO_2 spinel lattice. However, the electrolytically prepared $LiMn_2O_4$ with incomplete crystallization or extremely fine crystalline states will provide the Li^+/H^+ exchange path to the interior of the particle. This also serves as selectivity for the lithium-ion sieve property.

ACKNOWLEDGMENTS

The authors thank Elizabeth Behrens for helping potentiometric titration work; Roy Cahill for helping infrared absorption measurement; and also Roy Cahill and Boris Shpeizer for performing surface area determination of the electrolytically prepared manganese dioxide.

REFERENCES

1. J. B. Goodenough, M. M. Thackeray, W. I. F. David, and P. G. Bruce, *Rev. Chim. Minér.* **21,** 435 (1984).
2. M. M. Thackeray, P. J. Johnson, L. A. de Picciotto, P. G. Bruce, and J. B. Goodenough, *Mater. Res. Bull.* **19,** 179 (1984).
3. I. T. Sheftel and Ya. V. Pavlotskii, *Neorg. Mater.* **2,** 918 (1966).
4. M. M. Thackeray, W. I. F. David, P. G. Bruce, and J. B. Goodenough, *Mater. Res. Bull.* **18,** 461 (1983).
5. A. Mosbah, A. Verbaere, and M. Tournoux, *Mater. Res. Bull.* **18,** 1375 (1983).
6. W. I. F. David, M. M. Thackeray, L. A. de Picciotto, and J. B. Goodenough, *J. Solid State Chem.* **65,** 316 (1987).
7. M. M. Thackeray, A. de Kock, and W. I. F. David, *Mater. Res. Bull.* **28,** 1041 (1993).
8. M. M. Thackeray, A. de Kock, M. H. Rossouw, D. Liles, R. Bittihn, and D. Hoge, *J. Electrochem. Soc.* **139,** 363 (1992).
9. R. J. Gummow, A. de Kock, and M. M. Thackeray, *Solid State Ionics* **69,** 59 (1994).
10. R. Koksbang, J. Baker, H. Shi, and M. Y. Saidi, *Solid State Ionics* **84,** 1 (1996), and references therein.
11. V. V. Vol'khin, G. V. Leont'eva, and S. A. Onolin, *Neorg. Mater.* **6,** 1041 (1973).
12. X-M. Shen and A.Clearfield, *J. Solid State Chem.* **64,** 270 (1986).
13. G. V. Leont'eva and L. G. Chirkova, *Zh. Prikl. Khim.* **61,** 734 (1988).
14. K. Ooi, Y. Miyai, S. Katoh, H. Maeda, and M. Abe, *Langmuir* **5,** 150 (1989).
15. K. Ooi, Y. Miyai, S. Katoh, H. Maeda, and M. Abe, *Langmuir* **6,** 289 (1990).
16. K. Ooi, Y. Miyai, and J. Sakakihara, *Langmuir* **7,** 1167 (1991).
17. Q. Feng, Y. Miyai, H. Kanoh, and K. Ooi, *Langmuir* **8,** 1861 (1992).
18. J. C. Hunter, *J. Solid State Chem.* **39,** 142 (1981).
19. B. Ammundsen, D. J. Jones, J. Roziere, and G. R. Burns, *Chem. Mater.* **7,** 2151 (1995).
20. K. Sato, Y. Inoue, S. Yasukawa, and H. Takahashi, *Appl. Surf. Sci.* **65/66,** 308 (1993).
21. Y. Inoue, K. Sato, S. Yasukawa, and H. Takahashi, *in* "New Aspects of Spillover Effect in Catalysis" (T. Inui, Ed.), pp. 425–428. Elsevier, Amsterdam, 1993.
22. R. S. Yang, "Chemical Phase Analysis," pp. 76–78, Wiley, New York, 1974.
23. A. F. Daggett and W. B. Meldrum, "Quantitative Analysis," pp. 408–409. Heath, Boston, 1955.
24. A. Larson and R. B. Von Dreele, "Generalized Structure Analysis System," Los Alamos National Laboratory, Los Alamos, NM, 1994.
25. J. H. Scofield, *J. Electron Spectrosc.* **8,** 129 (1976).
26. *Nat. Bur. Stand.* (*U.S.*) *Monogr.* **25,** 1038 (1972); JCPDS card No. 24-734.
27. D. Briggs and J. C. Riviere, *in* "Practical Surface Analysis by Auger and X-ray Photoelectron Spectroscopy" (D. Briggs and M. P. Seah, Eds.), pp. 128–130, Wiley, New York, 1983.
28. J. A. Graham, W. M. Grim III, and W. G. Fateley, *in* "Fourier Transform Infrared Spectroscopy (J. R. Ferraro and L. J. Basile, Eds.), Vol. 4, pp. 345–392. Academic Press, Orlando, 1985.
29. H. Schmalzried, "Solid State Reactions," 2nd ed., pp. 104–110. Verlag Chemie, Weinheim, 1981.
30. A. F. Wells, "Structural Inorganic Chemistry," 5th ed., p. 545. Oxford Univ. Press, New York, 1984.
31. *Nat. Bur. Stand.* (*U.S.*) *Monogr.* **25,** 1195 (1973); JCPDS card No. 24-508.
32. F. Fillaux, C. H. Cachet, H. Ouboumour, J. Tomkinson, C. Levy-Clement, and L. T. Yu, *J. Electrochem. Soc.* **140,** 585 (1993).